

Nanomanufacturing of graphene nanosheets through nano-hole opening and closing

Yanan Chen ^{1,†}, Yilin Wang ^{1,†}, Shuze Zhu ², Kun Fu ¹, Xiaogang Han ¹, Yanbin Wang ¹, Bin Zhao ¹, Tian Li ¹, Boyang Liu ¹, Yiju Li ¹, Jiaqi Dai ¹, Hua Xie ¹, Teng Li ², John W. Connell ³, Yi Lin ^{4,*}, Liangbing Hu ^{1,*}

Facile and scalable fabrication of highly dense and high-quality graphene films and articles is extremely attractive for a range of electronic and mechanical applications. Pristine, high-quality graphene with its inherent impermeability poses challenges in fabricating dense films and thick parts with high electrical conductivity due to the difficulty in removing trapped air and/or solvents used in various fabrication methods. To overcome this deficiency, nano-holes were intentionally created in pristine graphene ("holey graphene") with an average diameter of approximately 15 nm. The holes serve as pathways for the rapid removal of gases or liquids and enable the fabrication of dense holey graphene nanostructures. Subsequently, a high-temperature process is applied to effectively repair the nano-holes and recover the high-quality graphene conjugated network. Through the creation and repair of the nano-holes, dense graphene articles that exhibited an ultrahigh conductivity of 2209 S/cm and superior thermal conductivity of 863 W/mK were created. This unique processing methodology enables the facile and scalable fabrication of high-quality graphene constructs, which can be easily integrated into the next generation of electronic circuits and high-power battery systems for highly efficient and lightweight thermal management.

Introduction

Graphene is an promising 2D material with excellent electrical conductivity [1], thermal conductivity [2], chemical and temperature resistance [3–6], mechanical strength, and low density [7] and is ubiquitously applied in fields, such as energy [8–14], environment [15,16], automobile, and aerospace [17]. However, the performance of graphene-based macrostructures (fibers, films, complex shapes, and articles), in terms of electrical conductivity and carrier mobility [18,19], is far less than that of an individu-

ally isolated high-quality graphene sheet. This is because the effects from the limit of lateral sizes of the sheets and the presence of defects become more significant with the size increase in the macrostructures. Also, the current approaches to fabricate graphene-based articles often introduce defects to enable the fabrication step, but those defects are difficult to fully remove and can diminish mechanical, electrical, and thermal properties. Current manufacturing methods for few-layer graphene or reduced graphene oxide (RGO) have a major limitation: difficulty in removing solvents or gases to achieve a dense structure, due to the impermeability of macroscopic stacks of such sheet-like 2D nanostructures. It has been reported that gases, such as H₂ and He, cannot permeate graphene nanosheets [20] and most

¹ Department of Materials Science and Engineering, University of Maryland College Park, College Park, MD 20742, United States

² Department of Mechanical Engineering, University of Maryland College Park, College Park, MD 20742, United States

³ Advanced Materials and Processing Branch, NASA Langley Research Center, Hampton, VA 23681-2199, United States

⁴ National Institute of Aerospace, 100 Exploration Way, Hampton, VA 23666-6147, United States

^{*} Corresponding authors.

E-mail addresses: Lin, Y. (yi.lin-1@nasa.gov), Hu, L. (binghu@umd.edu).

[†] Contributed equally to this work.

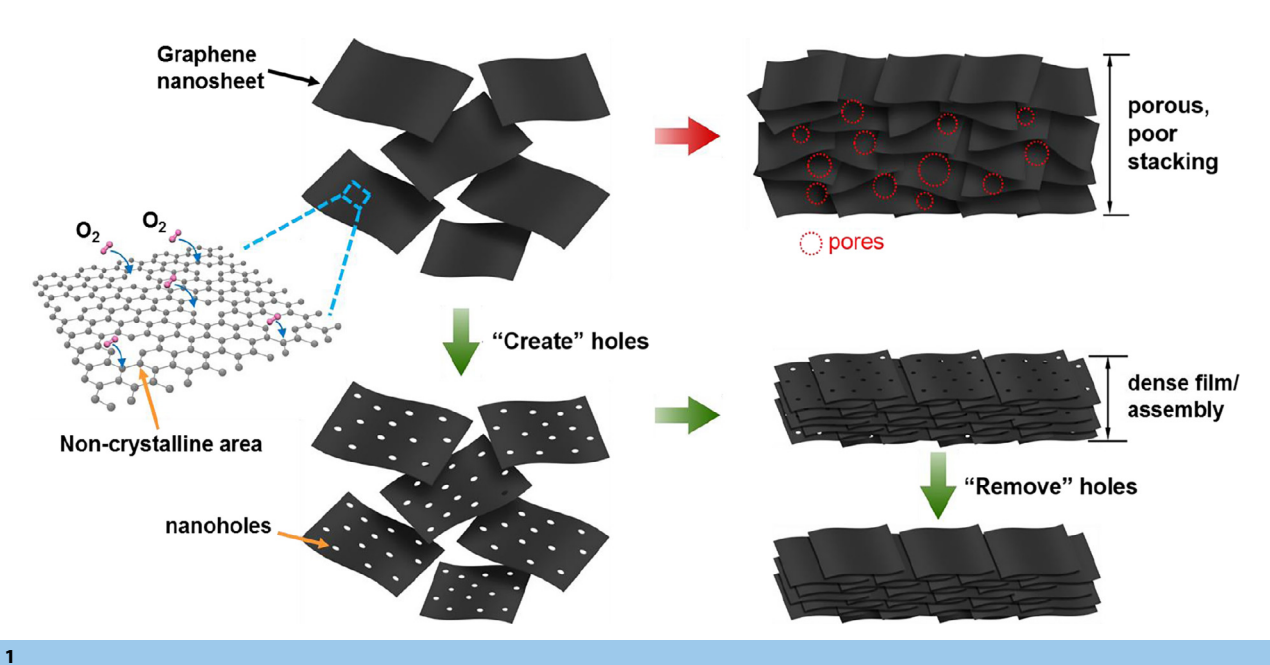


FIGURE 1

Schematic illustration of the process of opening and closing holes on few-layer graphene nanosheets to fabricate the highly dense and defect-free 2D graphene films and 3D graphene assemblies.

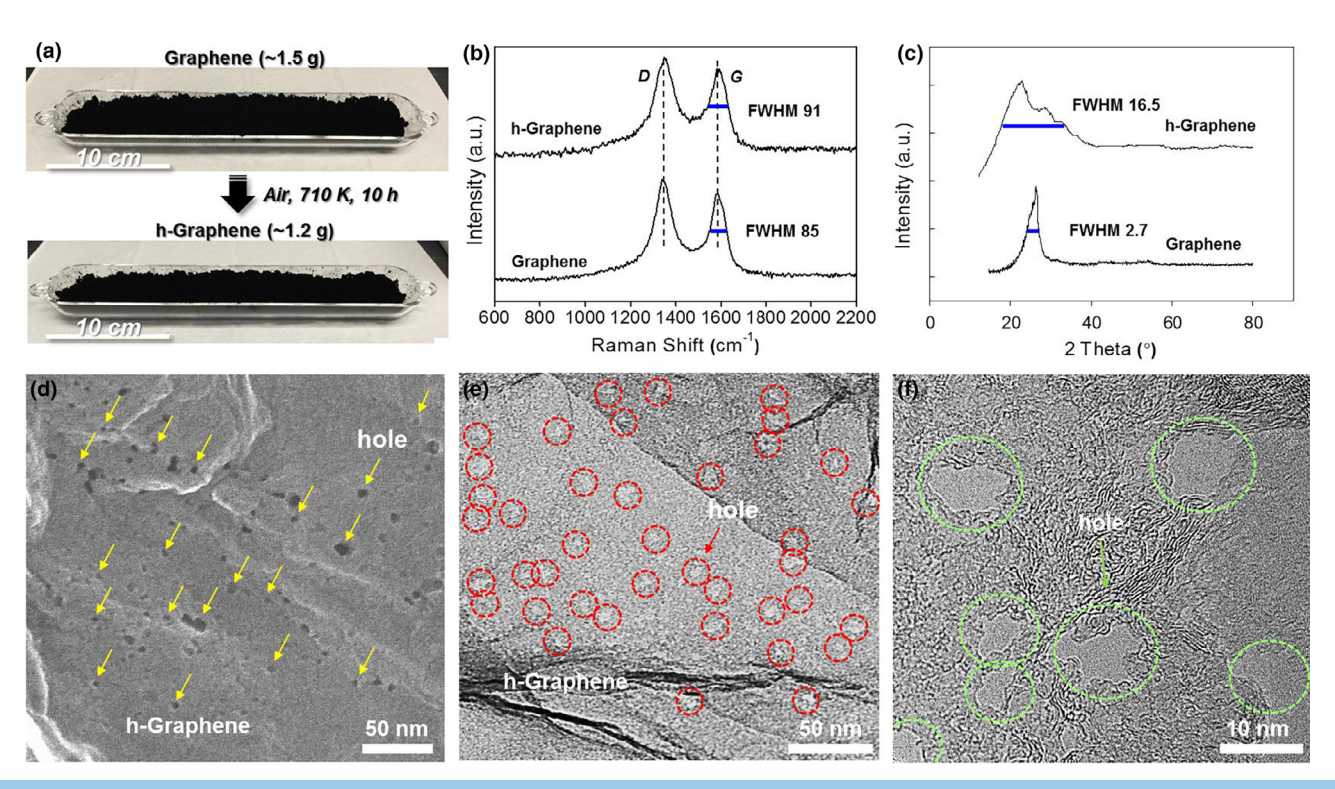


FIGURE 2

(a) One-step synthesis process of the h-Graphene nanosheets from commercial few-layer graphene nanosheets by heating at 710 K for 10 h in air. Shown in the photographs are the same sample before (top) and after (bottom) thermal treatment. (b) Raman spectra and (c) XRD patterns of pristine few-layer graphene and h-Graphene. (d) Typical SEM and (e) TEM images of few-layer h-Graphene nanosheets. (f) High-resolution TEM image of h-Graphene nanosheets. All images clearly show the nano-holes on the h-Graphene nanosheets. The holes are marked by yellow arrows (d), red circles (e), and green circles (f).

solvents cannot permeate intact graphene, which limits its effective manufacturing [20]. The electrical performance of graphene film fabricated from solution exfoliated few-layer graphene flakes

is poor, with a low DC conductivity on the order of 100 S/cm [21]. Another strategy for graphene manufacturing is to synthesize graphene oxide (GO), which allows for easier processing,

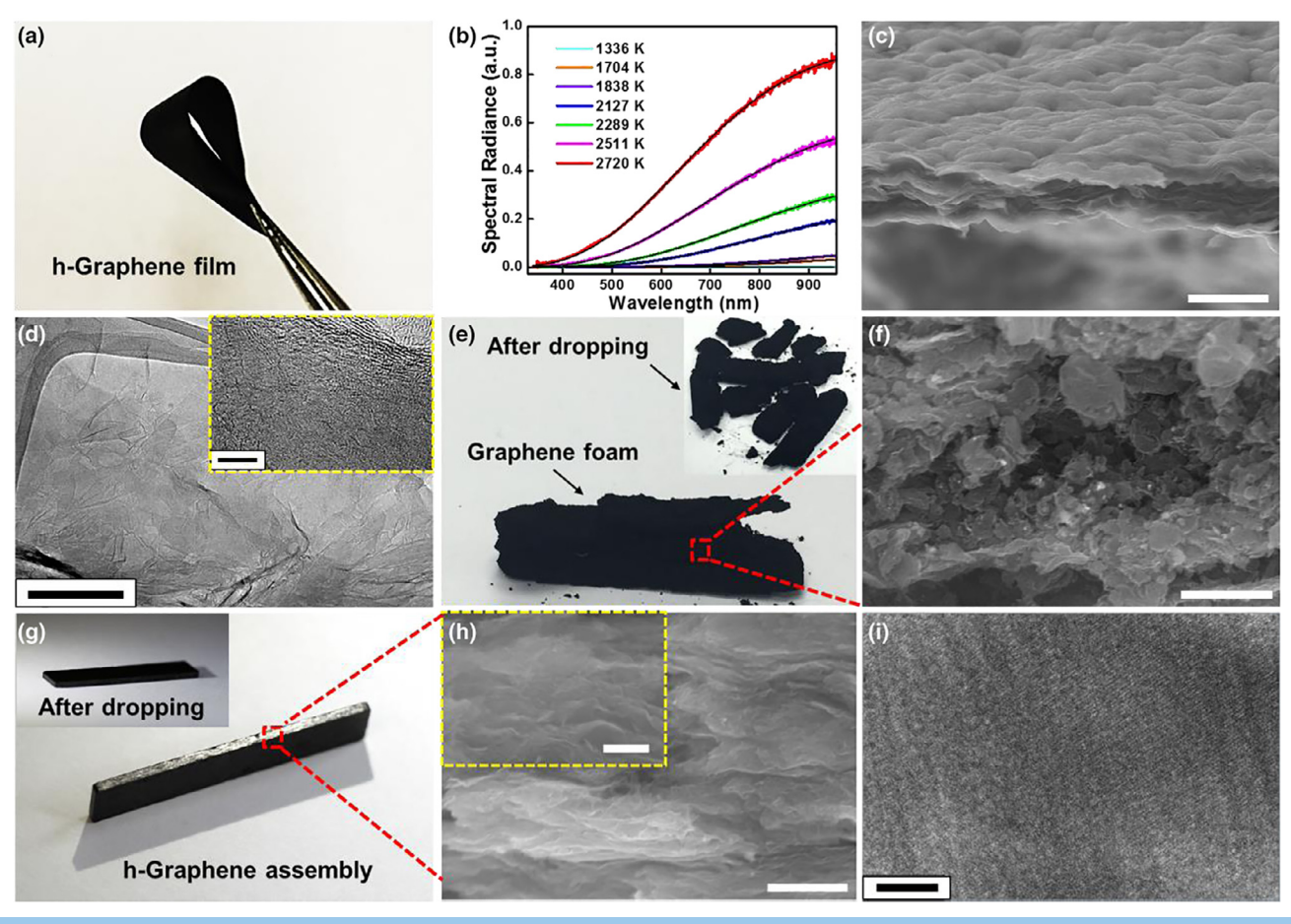


FIGURE 3

(a) Digital image of a flexible h-Graphene film fabricated by vacuum filtration. (b) Spectral radiance measurement of the same film sample at different bias voltages; the temperature was determined by fitting the spectra to Planck's law assuming constant emissivity. (c) SEM on the cross-sectional morphology of the 2700 K HT-treated h-Graphene film. Scale bar, 6 µm. TEM images at (d) lower and (inset) higher magnifications of the same 2700 K HT-treated h-Graphene film sample. Scale bar, 200 nm (d), 5 nm (inset). (e) Digital image of a dry-compressed assembly from the pristine graphene. Inset shows the damaged assembly after a 2-m height dropping test. (f) SEM image of the cross-sectional morphology of the graphene foam. Scale bar, 10 µm. (g) Digital image showing a dry-compressed h-Graphene bar assembly (length: 30 mm, width: 6 mm, thickness: 1 mm). Inset shows the survived assembly after a 2-m height dropping test. (h) SEM images of the cross-sectional morphology of the 2700 K HT-treated h-Graphene assembly. Inset shows the morphology at a higher magnification. Scale bar, 4 µm (h), 1 µm (inset). (i) HRTEM image of the same 2700 K HT-treated h-Graphene assembly. Scale bar, 5 nm.

followed by film fabrication, and then reduction [22-26]. Much higher conductivity has been demonstrated by the chemical reduction or thermal reduction in GO [27-35]. For example, the highest DC conductivity reported in chemically reduced graphene approaches 1000 S/cm [36]. Lian et al. recently reported that a high conductivity of 1790 S/cm was achieved for pure chemically converted graphene after thermal annealing under a high temperature up to 3123 K [37]. The solution processes discussed above to process the chemically converted graphene, typically via vacuum filtration, is time-consuming and has limitations with respect to film thickness. In addition, to achieve high electrical conductivity, the high-temperature annealing process requires expensive and complicated equipment, and is timeconsuming. Thus, developing a new methodology to scale-up and rapidly manufacture highly dense graphene architectures with excellent performance would be a major breakthrough.

Creating holes on the 2D material is an attractive approach as it is simple and scalable, and it solves the fundamental challenges in the ability to remove solvent and gas during article fab-

rication. The nano-holes enable the fabrication of dense nanostructures while also creating reactive edge sites for subsequent functionalization [38–41]. Recently, there has been much progress on the development and applications of holey graphene (h-Graphene) in energy storage (batteries, supercapacitors) [42–45], water desalination [46], and chemical and biosensing [47]. However, for applications requiring high electrical conductivity and thermal conductivity, the presence of holes in the final article is fundamentally problematic as they disrupt the graphitic conjugated network structure and deteriorate the original performance of high-quality graphene.

In this study, a facile, scalable process was demonstrated involving the creation of nano-holes on few-layer graphene nanosheets followed by rapid thermal healing to fabricate highly dense and defect-free 2D graphene films (via vacuum filtration) and 3D graphene assemblies (via dry compression molding), as illustrated in Fig. 1. Nano-holes on graphene nanosheets can be created by simply oxidizing commercial few-layer graphene powder in hot air to selectively oxidize defective sites. The

nano-holes allow for fast solvent escape when employing solution-processed methods, such as vacuum filtration. In addition, the as-obtained h-Graphene powders can be pressed or molded into an article under completely solvent-free conditions using a hydraulic press. After the solution-processed or drycompression fabrication, holes on the few-layer graphene nanosheets within the film or article can be rapidly closed or repaired by electrically induced thermal annealing, also known as "Joule heating", at high temperature (~2700 K). Different from traditional high-temperature treatment in a graphite furnace, Joule heating is fast, low-cost, and induces ultrahigh temperature at junction points between graphene nanosheets where higher electrical resistance exists. The self-healing thermal reduction makes it possible to form crosslinks between adjacent graphene nanosheets at the defects, which helps to build highly dense graphene structures, resulting in high electrical and thermal conductivities. Molecular dynamics (MD) modeling indicates that the hole closing or repairing mechanism involves the reconstruction of the conjugated carbon structure with carbon radicals filling up the holes under high temperature. The healed graphene architecture with closed holes exhibits excellent electrical conductivity (2209 S/cm), thermal conductivity (863 W/ mK), and superior mechanical strength.

The most common methods to create defects on graphene rely on the use of chemical methods, such as chemical etching with KOH and/or $\rm HNO_3$ and catalytic oxidation with metal or

metal oxide catalysts [43]. In this study, no conventional chemical methods are used for the hole creation or repair [38,42]. The simple one-step process to create holes on few-layer graphene is illustrated in Fig. 2a. In a typical reaction, ~ 1.5 g of commercial few-layer graphene powder was placed in a quartz boat and heated in an open-ended tube furnace at \sim 710 K with a heating rate of 10 K/min. After 10 h, ~1.1–1.2 g h-Graphene powder was obtained. The scalability of h-Graphene produced in this reaction is only limited by the size of the heating equipment. Mechanistically, the noncrystalline and defective sites on the pristine graphene nanosheets preferentially react with oxygen under hot air, leaving nano-holes. Raman spectral profiles of the pristine graphene and h-Graphene (Fig. 2b) display similar intensity ratio (~ 1.25) of the D band $(\sim 1350 \text{ cm}^{-1})$, defective carbon to G band $(\sim 1580 \text{ cm}^{-1})$, graphitic carbon). This suggests that almost the same amount of disordered carbon atoms are distributed on the few-layer graphene nanosheets despite the new presence of the nanosized holes. This result is consistent with the abovementioned mechanistic assumption of preferential defect carbon removal. The full width at half maximum (FWHM) of the G band of h-Graphene with a value of 94 reveals the deterioration of the overall crystal quality compared to that of graphene with a value of 85. XRD was employed to investigate the microstructure of the starting few-layer graphene and h-Graphene (Fig. 2c). The characteristic graphitic peak (26°) of h-Graphene was much broader with a FWHM of 16.5 compared with that of the pristine

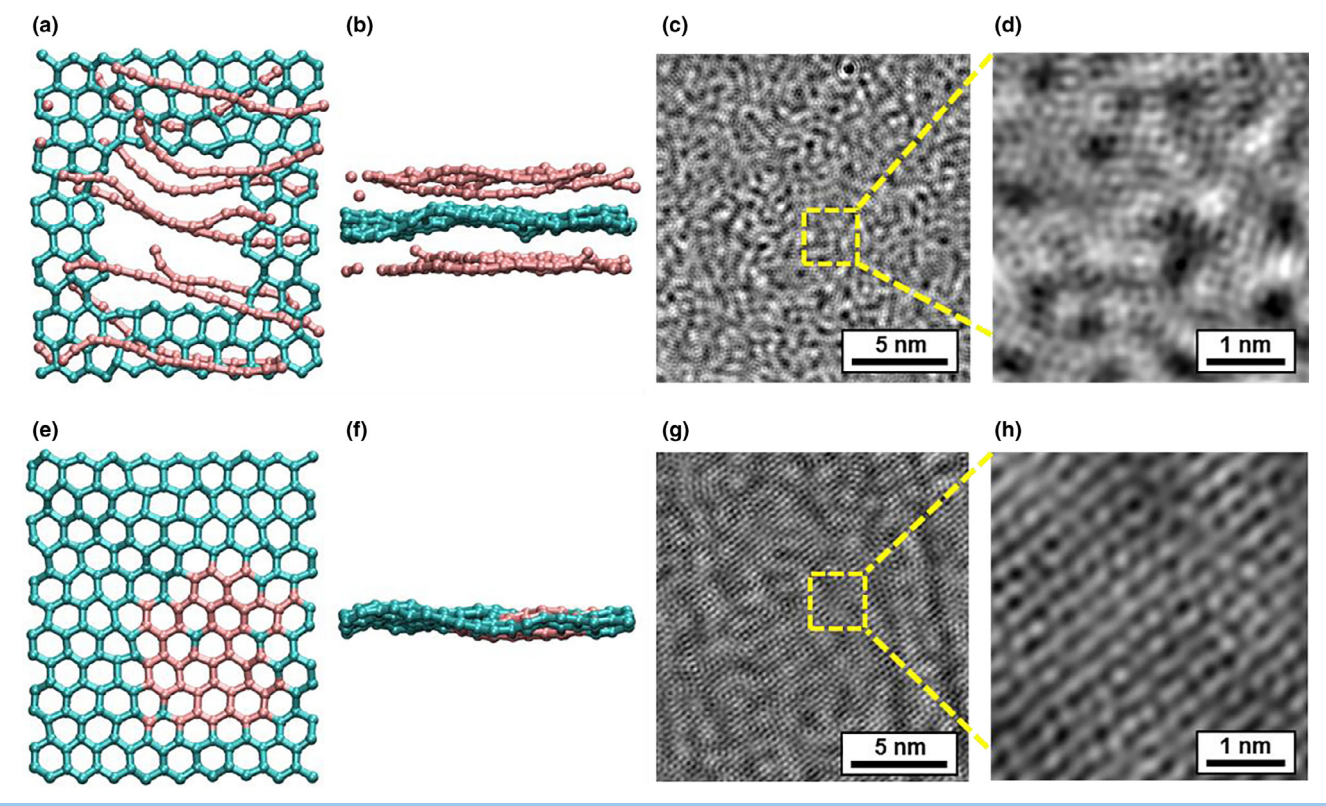


FIGURE 4

Molecular dynamics simulation results illustrating the carbon radicals filling in nano-holes in monolayer graphene at 2700 K. Cyan: carbon atoms that are initially from a monolayer graphene sheet with a nano-hole defect at the center. Pink: carbon radicals. (a) Top view before the hole defect is filled. (b) Side view of (a). (c, d) Filtered atomic-resolution TEM images of pristine h-Graphene. (e) Top view after the hole defect is filled. (f) Side view of (e). For visual clarity, the carbon radicals that have not filled the hole defect are not shown. (g, h) Filtered atomic-resolution TEM images of h-Graphene after 2700 K high-temperature treatment.

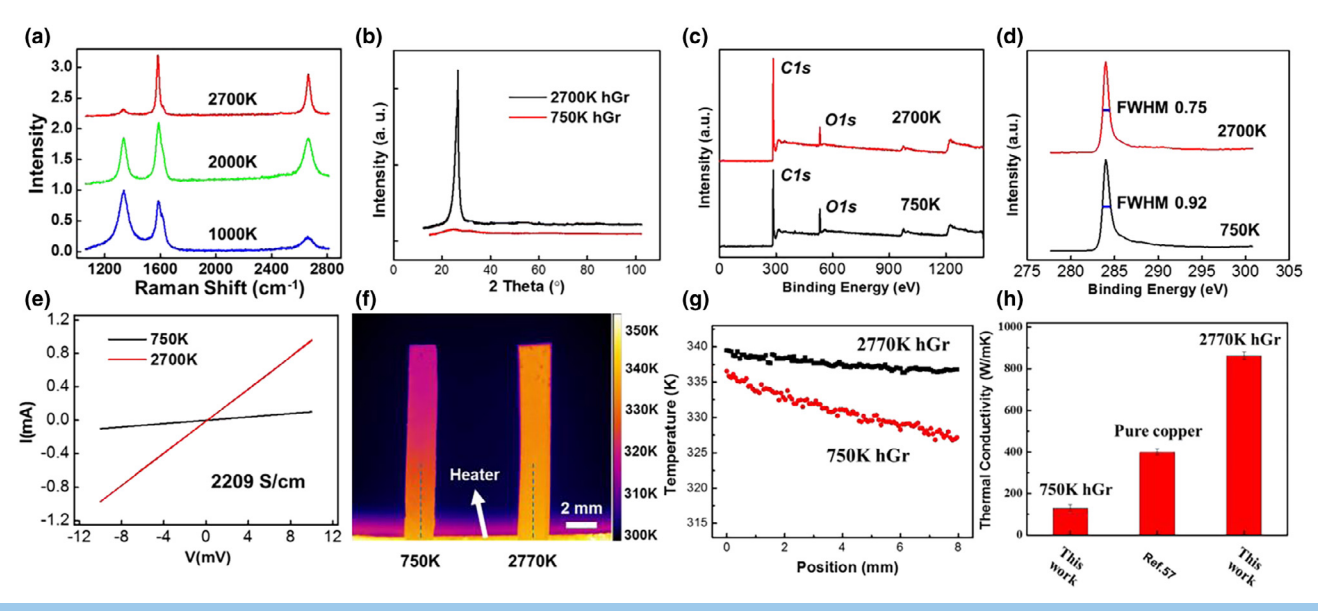


FIGURE 5

(a) Raman spectra of h-Graphene films that have been thermal treated at 1000 K, 2000 K and 2700 K respectively. (b) Representative XRD patterns, (c) XPS survey scans, and (d) C1s XPS spectra of a h-Graphene film before and after HT treatment at 2700 K. (e) *I–V* curves for a h-Graphene film before and after HT treatment at 2700 K. (f) A thermal infrared image showing rapid heat transport on the 2770 K HT-treated h-Graphene article in comparison with pristine h-Graphene. All samples were attached vertically on a microheater. The histogram on the right shows the color scale in accordance with the temperature. (g) Temperature profiles along the 2770 K h-Graphene and pristine h-Graphene from (f). (h) The thermal conductivity of 2770 K h-Graphene in comparison with pristine h-Graphene and pure copper.

graphene (2.7), indicating more disrupted stacking of the graphitic crystalline regions. The morphology of the pristine few-layer graphene nanosheets is illustrated in Figs. S1–S2, showing no holes on the graphene nanosheets before treatment (Supplementary Information). Fig. 2d shows a typical scanning electron microscopy (SEM) image of a few-layer h-Graphene nanosheet, indicating a large quantity of holes uniformly distributed on the nanosheet surface. These nano-holes are estimated to have an average diameter of 15 nm based on analysis of a large number of SEM and transmission electron microscopy (TEM) images acquired at different locations of the h-Graphene specimen (Fig. 2d–f).

The high-temperature (HT) thermal behavior of h-Graphene films and assemblies was investigated next. The free-standing h-Graphene film (~5 μm in thickness) with high flexibility (Fig. 3a) was fabricated by vacuum filtration of a few-layer h-Graphene dispersion (see details in Experimental Section). The film was then subjected to HT Joule heating by applying different bias voltages. Spectral radiance spectra of the heated film (Fig. 3b) were acquired in order to determine the actual film temperatures induced by the bias voltages. The spectra were then fit to Planck's law assuming constant emissivity (solid black curves in Fig. 3b), showing the achieved temperature range of \sim 1300–2700 K. Fig. 3c depicts the morphology of h-Graphene film after 2700 K HT treatment. Surprisingly, no obvious nano-holes can be found, and the graphene nanosheets seem to connect together into a continuous and smooth structure, this is in stark contrast to the as-prepared h-Graphene film as shown in Fig. 2d. Higher magnification image (Fig. S3) confirms the continuous graphene sheet without obvious nano-holes. TEM image shows that the HT-treated h-Graphene nanosheets (Fig. 3d) are similar to exfoliated few-layer graphene nanosheets from graphite [21], confirming the absence of nano-holes on HT-treated h-Graphene nanosheets. Higher magnification image displays the typical crystalline graphene lattice, indicating the high crystallization graphene structure from the 2700 K HT treatment (Inset in Fig. 3d).

Similar healing characteristics were also found on larger scale h-Graphene macrostructures or assemblies obtained from solvent-free dry compression. The starting graphene nanosheets were much less compressible due to the lack of an air escape mechanism during compression, as well as the resistance of the nanosheets to stacking together [38]. As shown in Fig. 3e, the assembly from the pristine graphene was only loosely bound with a low density ($\sim 0.1 \text{ g/cm}^3$) after dry pressing and easily broke into pieces after a 2-m height dropping test (inset in Fig. 3e). The cross-sectional SEM image confirms the random arrangement of pristine graphene flakes with many large voids in between, resulting in a low packing density (Fig. 3f). The h-Graphene assembly with a predefined bar shape (length: 30 mm, width: 6 mm, thickness: 1 mm) was obtained by pressing h-Graphene nanosheets in the designed mold under completely solvent-free conditions (Fig. 3g). The fabricated h-Graphene assembly exhibited excellent mechanical stability, retaining the shape after both 2-m height dropping test and HT treatment (inset in Fig. 3g). The cross-sectional SEM image of the 2700 K HT-treated h-Graphene assembly showed that the graphene layers were closely packed (Fig. 3h), enabling good contacts among the laterally aligned graphene nanosheets across the entire vertical direction. HRTEM image confirms the high crystallization structure without nano-holes of 2700 K HT-treated h-Graphene (Fig. 3i). The tight packing and inter-contacting structure led to

a highly dense graphene assembly (\sim 1.5 g/cm³) and induced a continuous pathway for electrons and phonons to transport efficiently, resulting in greatly improved electrical conductivity and thermal conductivity.

Based on the experimental and modeling results, we propose a "hole-filling" mechanism that the high temperature of 2700 K, the nano-holes can be filled in by carbon radicals in the local environment. MD simulations were applied to investigate the hole-filling (carbon atoms reconstruction) behavior in a system where initially there is a monolayer graphene with a hole defect and a number of dispersed carbon radicals (Fig. 4a, b). The simulation was maintained at 2700 K (simulation details and extended data are shown in Figs. S4-S5, Supplementary Information). The hole was observed to be filled by carbon radicals after 175 ps (Fig. 4e, f). The above modeling results agree with recent reports on defect healing [48,49]. The structural evolution of the h-Graphene during high-temperature treatment was also investigated by TEM on the atomic scale. The majority of the pristine h-Graphene TEM image displays short-range order, as shown in Fig. 4c. The detailed image (Fig. 4d) clearly shows the disordered features organized from small domains, which are ascribed to the presence of defects on h-Graphene. The filtered atomic-resolution TEM images of 2700 K HT-treated h-Graphene architecture reveals the highly ordered honeycomb structure, verifying the carbon atoms reconstruction derived from h-Graphene during the high-temperature treatment process (Fig. 4g, h).

The intrinsic structure and chemical compositions of h-Graphene after HT treatment were investigated to understand the process of creating and repairing holes on few-layer graphene nanosheets. Fig. 5a shows Raman spectra of three HT-treated h-Graphene films under different temperatures (1000 K, 2000 K, 2700 K) for comparing the structure evolution upon heating. G band (\sim 1580 cm⁻¹) and 2D band (\sim 2700 cm⁻¹), both related to crystalline graphitic structures, were clearly visible under all conditions. However, the D bands (~1350 cm⁻¹), an indicator of defects, were only apparent with strong intensity in the cases of h-Graphene films treated at 1000 K and 2000 K, with D-to-G ratio (I_D/I_G) of 1.2 and 0.75, respectively. For the case of 2700 K HT-treated h-Graphene film, the D peak intensity was very low with an I_D/I_G ratio of 0.11, indicating the highly crystalline structure. These Raman spectra suggest that the 2700 K HT-treated h-Graphene closely approach defect-free graphene, and the very weak D peak may be caused by the edge effects and the negligible functional groups. X-ray diffraction (XRD) was employed to investigate the layered structure and d-spacing of 2700 K h-Graphene (HT treated, closed holes) and the as-prepared h-Graphene (open holes). 2700 K HT-treated h-Graphene exhibited a sharp peak at \sim 26.55°, while the as-prepared h-Graphene only showed a broad peak at ~24.98°, consistent with the high graphitic crystallinity induced by HT Joule heating (Fig. 5b). It is worth noting that the *d*-spacing (d = 0.357 nm) of the asprepared h-Graphene decreases to 0.335 nm after 2700 K treatment, very near the value of graphite (~0.334 nm), which suggests the dense stacking of h-Graphene nanosheets with closed holes after high-temperature treatment. X-ray photoelectron spectral (XPS) studies revealed that the C/O atomic ratio of h-Graphene significantly increased from 8.53 to 16.54 after

2700 K HT treatment (Fig. 5c), indicating the effective removal of oxygen functional groups existing on h-Graphene. The FWHM of the high-resolution C 1s XPS spectra of 2700 K treated h-Graphene (0.75 eV) is narrower than that of the as-prepared sample (0.92 eV), further confirming the improved crystallinity after 2700 K HT treatment (Fig. 5d).

The 2700 K HT-treated h-Graphene film (thickness $\sim 5 \mu m$) with closed holes achieved an ultrahigh room temperature electrical conductivity of 2209 S/cm. As shown in the I-V curves of a h-Graphene sample tested at room temperature (Fig. 5e), the electrical conductivity of h-Graphene increases from \sim 128 S/ cm to ~ 2209 S/cm after 2700 K HT treatment, an improvement of ~17-fold. Hall measurement of the HT-treated h-Graphene with closed holes confirmed the ultrahigh conductivity, and the excellent transport characteristics as indicated by the high carrier mobility of 673 cm² V⁻¹ s⁻¹ with a carrier density of $2.18 \times 10^{19} \, \text{cm}^{-3}$. In comparison, as-prepared h-Graphene exhibited much lower carrier mobility (26 cm² V⁻¹ s⁻¹) and carrier density $(3.3 \times 10^{19} \text{ cm}^{-3})$ (Fig. S5a-b, Supplementary Information). The carrier mobility and density of the h-Graphene is dominated by impurities/defects of the h-Graphene nanosheets, with the lower the amount of impurities/defects, the larger the carrier mobility and the smaller the carrier density. Thus, the enhanced carrier mobility and decreased carrier density of HTtreated h-Graphene mainly contribute to the repair of holes, removal of defects, and restoration of the conjugated network of the h-Graphene nanosheets via high-temperature annealing, as confirmed by the Raman, XRD, and XPS spectra shown in Fig. 5a-d. The aforementioned carrier mobility of h-Graphene with closed holes is among the highest carrier mobilities of state-of-the-art graphene films composed with single-layer or few-layer graphene flakes. Typical carrier mobility values for graphene films are usually between 0.1 and 372 cm² V⁻¹ s⁻¹, as reported in the literature (Fig. S5c, Supplementary Information) [50-55].

The thermal conductivity of the HT-treated h-Graphene architecture was investigated using a steady-state method. The thermal infrared images of the 2770 K HT-treated h-Graphene article and the pristine h-Graphene article (Fig. 5f) show that the temperature distribution of the HT-treated h-Graphene is much more uniform than that of the pristine h-Graphene, in which the high-temperature area was mainly concentrated at the contact area, illustrating the faster heat-transfer speed of HT-treated h-Graphene. The temperature profiles reveal that HT-treated h-Graphene exhibits higher temperature than that of the pristine h-Graphene at the same position (Fig. 5g), indicating the improved thermal conductive capability of HT-treated h-Graphene. According to the well-established thermal conductive model [56] (Fig. S7, Supplementary Information), the thermal conductivity of HT-treated h-Graphene reaches 863 W/mK, which is 7-times higher than the pristine h-Graphene article and 2-times higher than pure copper [57] (Fig. 5h). The excellent thermal conductivity of HT-treated h-Graphene should originate from the large area and high-quality graphene conjugated network formed by effective healing of the defects, nano-holes, and grain boundaries, enabling efficient phonon diffusion from lattice vibrations of the sp²-bonding network. The rapidly increasing power density in electronics requires excellent

thermal management materials with not only high thermal conductivity but also high thermal throughput. It is worth noting that the thickness of the HT-treated h-Graphene article is about 2 orders of magnitude higher than reported graphene films or commercial thermal conductive films with typical thicknesses of 10–20 µm [58,59]. Therefore, the thermal transfer capacity of the HT-treated h-Graphene article should be 2 orders of magnitude higher than films with the same thermal conductivity. The excellent thermal conductivity and the merits in thickness of up to millimeter scale suggest our HT-treated h-Graphene articles as highly efficient and lightweight thermal management bulk materials for the next generation of integrated circuits and high-power battery systems spanning from smartphones, tablet PCs, electric cars to the aerospace industry (e.g., aircrafts, satellites, and rockets).

Conclusion

In this study, we demonstrated that heating graphene nanosheets in hot air resulted in the creation of nano-holes, which can be subsequently repaired after being treated at HT of 2700 K. The h-Graphene can be fabricated into dense films by solution-based process (i.e., vacuum filtration) due to fast solvent escape through the holes on graphene nanosheets. The h-Graphene can even be directly compressed into a dense assembly under completely solvent-free conditions, opening up a new strategy for fast manufacturing of high-quality graphene based architectures. The highly dense graphene film or assembly with holes can be transformed to hole-free, highly crystalline graphene architecture after fast HT treatment via Joule heating. The HT-treated h-Graphene exhibits excellent electron and phonon transport characteristics with ultrahigh electrical conductivity of 2209 S/cm and superior thermal conductivity of 863 W/ mK. The proposed mechanism of repairing the nano-holes and recovering the conjugated network of the graphene nanosheets, as supported by MD modeling, is that carbon atoms recombine and carbon radicals fill in the holes under high temperature, creating a near-perfect carbon lattice consistent with that of graphene. We envision that this strategy of creating and repairing holes on graphene nanosheets utilizing thermal treatment provides new tools to tune defects on graphene for applications, such as separation, sensors, and transistors, and a new route to rapidly manufacture graphene materials with ultrahigh electrical and thermal conductivity, which are invaluable properties for the next generation of integrated circuits and high-power battery systems in smartphones, tablet PCs, electric cars, and the aerospace industry.

Acknowledgments

L.H. and Y.C. acknowledge the support of NSF grants (1635221). We acknowledge the support of the Maryland NanoCenter and its NispLab. Y.L. and J.W.C acknowledge the financial support from the NASA Langley Internal Research and Development (IRAD) Program.

Appendix A. Supplementary data

Supplementary data associated with this article can be found, in the online version, at https://doi.org/10.1016/j.mattod.2018.09.

References

- [1] A.K. Geim, K.S. Novoselov, Nat. Mater. 6 (2007) 183.
- [2] A.A. Balandin et al., Nano Lett. 8 (2008) 902.
- [3] Y. Chen et al., Nat. Commun. 7 (2016) 12332.
- [4] B. Wang et al., ACS Nano 10 (2016) 9794.
- [5] Y. Yao et al., ACS Nano (2016).
- [6] Y. Chen et al., Nano Lett. 16 (2016) 5553.
- [7] C. Lee et al., Science 321 (2008) 385.
- [8] X. Xie et al., Energy Environ. Sci. 5 (2012) 6862.
- [9] D. Lin et al., Nat. Nanotechnol, 11 (2016) 626.
- [10] H. Wang et al., Energy Environ. Sci. 5 (2012) 7931.
- [11] N. Li et al., Proc. Natl. Acad. Sci. 109 (2012) 17360.
- [12] F. Bonaccorso et al., Science 347 (2015) 1246501.
- [13] Y. Zhu et al., Adv. Mater. 22 (2010) 3906.
- [14] H. Chen et al., Adv. Mater. 29 (2017) n/a.
- [15] N. Liu et al., Nano Lett. 14 (2014) 3702.
- [16] Y. Li et al., J. Am. Chem. Soc. 133 (2011) 7296.
- [17] Z. Chen et al., Adv. Mater. 25 (2013) 1296.
- [18] Y. Liu et al., ACS Nano 11 (2017) 4301. [19] Y. Liu et al., Adv. Mater. 28 (2016) 7941.
- [20] Y. Su et al., Nat. Commun. 5 (2014) 5843.
- [21] X. Han et al., Nanotechnology 24 (2013) 205304.
- [22] Y.L. Zhong et al., Mater. Today 18 (2015) 73.
- [23] H. Chen et al., Adv. Mater. 20 (2008) 3557.
- [24] D.R. Dreyer et al., Chem. Soc. Rev. 39 (2009) 228.
- [25] D. Li et al., Nat. Nanotechnol. 3 (2008) 101.
- [26] D. Li, R.B. Kaner, Science 320 (2008) 1170.
- [27] Z. Li et al., Nat. Commun. 7 (2016) 13684.
- [28] Z. Xu et al., Adv. Mater. 28 (2016) 6449.
- [29] Z.-S. Wu et al., ACS Nano 3 (2009) 411.
- [30] Z. Xu et al., ACS Nano 6 (2012) 7103.
- [31] S. Park, R.S. Ruoff, Nat. Nanotechnol. 5 (2010) 309.
- [32] I.K. Moon et al., Nat. Commun. 1 (2010) 73.
- [33] A. Bagri et al., Nat. Chem. 2 (2010) 581.
- [34] L.J. Cote, R. Cruz-Silva, J. Huang, J. Am. Chem. Soc. 131 (2009) 11027.
- [35] S. Pei et al., Carbon 48 (2010) 4466.
- [36] S. Pei, H.-M. Cheng, Carbon 50 (2012) 3210.
- [37] G. Xin et al., Science 349 (2015) 1083.
- [38] X. Han et al., ACS Nano 8 (2014) 8255.
- [39] L. Jiang, Z. Fan, Nanoscale 2014 (1922) 6.
- [40] H. Li et al., Adv. Mater. 28 (2016) 8945.
- [41] Y. Ito et al., Adv. Mater. 28 (2016) 10644.
- [42] Y. Lin et al., Adv. Funct. Mater. 25 (2015) 2920.
- [43] Y. Lin et al., Nanoscale 5 (2013) 7814.
- [44] H. Sun et al., Science 356 (2017) 599.
- [45] Y. Xu et al., Nat. Commun. 5 (ncomms555) (2014) 4.
- [46] S.P. Surwade et al., Nat. Nanotechnol. 10 (2015) 459.
- [47] S.J. Heerema, C. Dekker, Nat. Nanotechnol. 11 (2016) 127.
- [48] A. Barreiro et al., Sci. Rep. (2013) 3.
- [49] A. Barreiro et al., Nano Lett. 2012 (1873) 12.
- [50] G. Eda, G. Fanchini, M. Chhowalla, Nat. Nanotechnol. 3 (2008) 270.
- [51] S. Wang et al., Adv. Mater. 20 (2008) 3440.
- [52] G. Eda, M. Chhowalla, Nano Lett. 9 (2009) 814.
- [53] S. Wang et al., Nano Lett. 10 (2010) 92.
- [54] R. Negishi, Y. Kobayashi, Appl. Phys. Lett. 105 (2014) 253502.
- [55] A. Bhaumik et al., J. Mater. Sci. Eng. 6 (2017) 1.
- [56] H. Zhu et al., ACS Nano 8 (2014) 3606.
- [57] A.A. Balandin, Nat. Mater. 10 (2011) 569.
- [58] Z.-L. Hou et al., ACS Appl. Mater. Interfaces 6 (2014) 15026.
- [59] M. Zhang et al., Adv. Mater. 27 (2015) 6708.